remote sensing

MDPI

Article

Fast and Accurate Collocation of the Visible Infrared Imaging Radiometer Suite Measurements with Cross-Track Infrared Sounder

Likun Wang [1,*], Denis Tremblay [2], Bin Zhang [3] and Yong Han [4]

Received: 29 November 2015; Accepted: 18 January 2016; Published: 21 January 2016
Academic Editors: Changyong Cao, Dongdong Wang and Prasad S. Thenkabail

1 Earth System Science Interdisciplinary Center, University of Maryland, 5825 University Research Court, Suite 4001, College Park, MD 20740, USA
2 Science Data Processing Inc., Laurel, MD 20723, USA; Denis.Tremblay@noaa.gov
3 Earth Resource Technology Inc., 14401 Sweitzer Lane, Laurel, MD 20707, USA; Bin.Zhang@noaa.gov
4 Center for Satellite Applications and Research, NESDIS/NOAA, 5830 University Research Court, College Park, MD 20740, USA; Yong.Han@noaa.gov
* Correspondence: wlikun@umd.edu; Tel.: +1-301-683-3551; Fax: +1-301-405-8468

Abstract: Given the fact that Cross-track Infrared Sounder (CrIS) and the Visible Infrared Imaging Radiometer Suite (VIIRS) are currently onboard the Suomi National Polar-orbiting Partnership (Suomi NPP) satellite and will continue to be carried on the same platform as future Joint Polar Satellite System (JPSS) satellites for the next decade, it is desirable to develop a fast and accurate collocation scheme to collocate VIIRS products and measurements with CrIS for applications that rely on combining measurements from two sensors such as inter-calibration, geolocation assessment, and cloud detection. In this study, an accurate and fast collocation method to collocate VIIRS measurements within CrIS instantaneous field of view (IFOV) directly based on line-of-sight (LOS) pointing vectors is developed and discussed in detail. We demonstrate that this method is not only accurate and precise from a mathematical perspective, but also easy to implement computationally. More importantly, with optimization, this method is very fast and efficient and thus can meet operational requirements. Finally, this collocation method can be extended to a wide variety of sensors on different satellite platforms.

Keywords: VIIRS; CrIS; inter-calibration; collocation; cloud detection

1. Introduction

The Suomi National Polar-orbiting Partnership (Suomi NPP) satellite, successfully launched in October 2011, is a weather satellite to serve as a gap-filler between NOAA's heritage Polar Operational Environmental Satellites (POES) and the new generation Joint Polar Satellite Systems (JPSS). Five key instruments are carried on Suomi NPP, that is, the Advanced Technology Microwave Sounder (ATMS), the Cross-track Infrared Sounder (CrIS), the Ozone Mapping and Profiler Suite (OMPS), the Visible Infrared Imaging Radiometer Suite (VIIRS), and Clouds and the Earth's Radiant Energy System (CERES). Among them, VIIRS is a whiskbroom scanning imaging radiometer, collecting visible and infrared imagery of the Earth through 22 spectral bands between 0.412 μm and 12.01 μm with a resolution of 375 m or 750 m at nadir [1]. CrIS is a Michelson interferometer with 1305 spectral channels over three wavelength ranges: long-wave infrared (LWIR) (9.14–15.38 μm), middle-wave IR (MWIR) (5.71–8.26 μm), and short-wave IR (SWIR) (3.92–4.64 μm) [2]. In contrast to a state-of-the-art high-spatial-resolution imager instrument of VIIRS, the sounder instrument CrIS provides information on the vertical profiles of temperature, water vapor, and critical trace gases of the atmosphere,

albeit with coarse spatial resolution (14.0 km at nadir). The combination of high spatial resolution measurements from an imager and high spectral resolution measurements from an infrared (IR) sounder can take advantage of both spectral and spatial capabilities; hence, it can further improve atmospheric and surface geophysical parameter retrievals [3,4] and data utilization for numerical weather prediction models [5]. Furthermore, owing to its hyperspectral nature and accurate radiometric and spectral calibration, radiance spectra from the IR sounder can be integrated through the spectral response functions (SRF) to simulate imager radiance measurements and thus independently assess spectral and radiometric calibration accuracy of IR channels of the imager [6–10]. Finally, recent study demonstrated that, by taking advantage of high spatial resolution and accurate geolocation of VIIRS measurements, spatially collocated measurements from the VIIRS image bands can effectively evaluate the geolocation accuracy of CrIS that has a coarse spatial resolution [11]. All these applications are dependent on accurate and fast collocation of sounder measurements with imager measurements.

Collocation of the measurements from two satellite sensors (either on the same satellite platform or not) involves pairing measurements from two sensors that observe the same location on the Earth but with different spatial resolutions. In other words, it involves finding overlapped measurements from two sensors. After this step, the observational time and atmospheric path (e.g., satellite zenith and azimuth angle differences) of paired and collocated measurements can be further checked by constraining the observational time and view geometry differences dependent on applications. For the two sensors on the same platform, time and angle difference is not an issue. For two sensors on different platforms, once the first step is accomplished, it is relatively easy to further filter the data by choosing suitable thresholds of time and angle differences. For both cases, spatial collocation is the key step. Therefore, the collocation in this study is mainly referred to as spatial collocation that associates overlapped measurements from two sensors.

To the best of our knowledge, not many studies have been published on spatial collocation methods in existing literature. A traditional but simple method is to check ground pixel distance to find overlapped measurements [12,13]. This method cannot precisely and accurately deal with off-nadir field of view (FOV) distortion because the FOV footprint projected on the ground becomes egg-shaped, or oviform as the scan moves away from nadir. As a pioneer study, Aoki (1980) [14,15] describes how to match AVHRR and HIRS/2 on the same satellite. The first peer-reviewed publication on spatial collocation is the work by Nagle and Holz (2009) [16], which provides a guidance for a general methodology that can be applied to a wide range of satellite, aircraft, and surface measurements and allow for efficient collocation with measurements having varying spatial and temporal sampling. Specifically, two methods are discussed for spatial collocation (referred to as "overlap detection" in the paper), including (1) the quasi-elliptical approach and (2) the quasi-conical approach. The quasi-elliptical approach basically assumes that the projected footprints on the Earth Surface from the sounder's FOVs are approximately elliptical. A coordinate system based on the major and minor axes of the quasi ellipse are created on the terrestrial surface. The collocation task is then simplified to determine whether a given point on the Earth's surface falls within the quasi ellipse by examining the distance to the major and minor axes. By contrast, the quasi-conical approach avoids any exercise in analytic geometry and is much more straightforward. Basically, any sounder instrument views the underlying Earth as if through a cone whose angular opening is determined by the size of the FOV angle. Then, the imager observation viewed within the solid angle of the cone overlaps the sounder FOV on the ground. Compared to the quasi-elliptical approach method, one need not be concerned with the size, shape, or orientation of the FOV projected on the surface. In both studies by Aoki (1980) [14] and Nagle and Holz (2009) [16], the quasi-elliptical approach has been described in detail and thus recommended for use, while the second method—the conical approach—is not suggested by Nagle and Holz (2009) because of its computational inaccuracy for small angles [16]. However, for hyperspectral IR instruments like CrIS, which contains 3×3 detectors in one field of regards (FOR), the corresponding FOV footprints are rotated along with scan positions due to the 45°-mounted scan mirror, resulting in complicated geometric calculations. In addition, the quasi-elliptical approximation

inevitably causes uncertainties owing to a perceptible curvature of the Earth when the scan angle increases. For applications that require accurate spatial collocation (e.g., geolocation assessment), the first approach is inadequate.

In this study, we argue that the conical approach is accurate and precise in essence and much easier to apply in computation algorithms. With appropriate optimization, this method is not only fast and efficient but also can meet accuracy requirements. Finally, given the fact that CrIS and VIIRS will continue to be onboard the same platform of future Joint Polar Satellite System (JPSS) satellites for the next decade, it is desirable to discuss the implementation details of spatial collocation between CrIS and VIIRS to assist applications that rely on the combination of measurements from two sensors. More importantly, as we demonstrate later, without loss of generality, this collocation method can also be applied to a wide variety of sensors on different satellites.

The paper is organized as follows: Section 2 summarizes instruments of characteristics, Section 3 describes the methodology, Section 4 presents the results and applications and Section 5 concludes the paper.

2. Instrument Characteristics

Both CrIS and VIIRS are onboard Suomi NPP spacecraft at a nominal altitude of ~829 km in a Sun-synchronous orbit with local equatorial crossing times of ~13:30 (ascending) and ~01:30 A.M (descending). As a step-scan Fourier transform spectrometer, CrIS takes 8 s for each scan sweep, each collecting 34 Fields of Regard (FORs). Among them, 30 are the Earth scenes and four are the embedded space and blackbody calibration views. The scan mirror stepwise "stares" at the Earth step by step in the cross-track direction from -48.3° to +48.3 with a 3.3° step angle, equaling a 2200 km swath width on the Earth. Nine field stops define the 3×3 detector array for each IR wavelength band, which are arrayed as 3×3 0.963° circles and separated by 1.1°. CrIS radiance spectrum (without apodization) covers three IR bands from 650 to 1095 cm^{-1}, 1210 to 1750 cm^{-1}, and 2155 to 2550 cm^{-1} with spectral resolutions of 0.625 cm^{-1}, 1.25 cm^{-1}, and 2.5 cm^{-1} at the normal operational mode (a total of 1305 spectral channels). After apodization by using a Hamming function, the effective spectral resolution decreases by a factor of 1.82.

The VIIRS instrument is a whiskbroom scanning radiometer with a field of regard of $\pm 56.3^\circ$ in the cross-track direction. The swath width is 3060 km. VIIRS has 22 spectral bands covering the spectrum between 0.412 μm and 12.01 μm, including 16 moderate resolution bands (M-bands) with a spatial resolution of 750 m at nadir, 5 imaging resolution bands (I-bands)–375 m at nadir, and 1 panchromatic Day-Night-Band (DNB) with a 750 m spatial resolution throughout the scan. The M-bands include 11 Reflective Solar Bands (RSB) and 5 Thermal Emissive Bands (TEBs). The I-bands include three RSBs and two TEBs. VIIRS uses a unique approach of pixel aggregation which controls the pixel growth towards the end of the scan. As a result, the VIIRS spatial resolutions for nadir and edge-of-scan data are comparable. For example, for typical I-bands, the resolution changes from 375 m at nadir to ~800 m at the end of a scan. On the other hand, in order to save transmission bandwidth, VIIRS also uses a "bow-tie removal" approach that removes duplicated pixels in the off-nadir areas where there is an overlap of several pixels between adjacent scans [1].

There are four VIIRS IR channels that are fully covered by CrIS spectra at the longwave IR (LWIR) and shortwave IR (SWIR) bands as shown in Figure 1, including three M-bands and one I-band, *i.e.*, M13 (4.05 μm) , M15 (10.8 μm) , M16 (12.0 μm), and I5 (11.5 μm). In this study, we only use high spatial resolution VIIRS I5 data. However, the method proposed in this study can also be applied to other bands and VIIRS product. In order to compare CrIS hyperspectral radiances with VIIRS band radiances, we need to perform spectral convolution to reduce the high resolution CrIS spectrum to match the band radiances from VIIRS. Specifically, given the CrIS hyperspectral radiance R at each

wavenumber, it can be convolved with the VIIRS SRF S to generate the CrIS-convolved VIIRS band radiance L as

$$L = \frac{\int_{\nu_1}^{\nu_2} R(\nu)S(v)d\nu}{\int_{\nu_1}^{\nu_2} S(\nu)d\nu} \quad (1)$$

where ν_1 and ν_2 are band pass limits. Henceforward, except for those specially noted below, the CrIS data in this study are referred to as the simulated VIIRS band radiances for the I5 band.

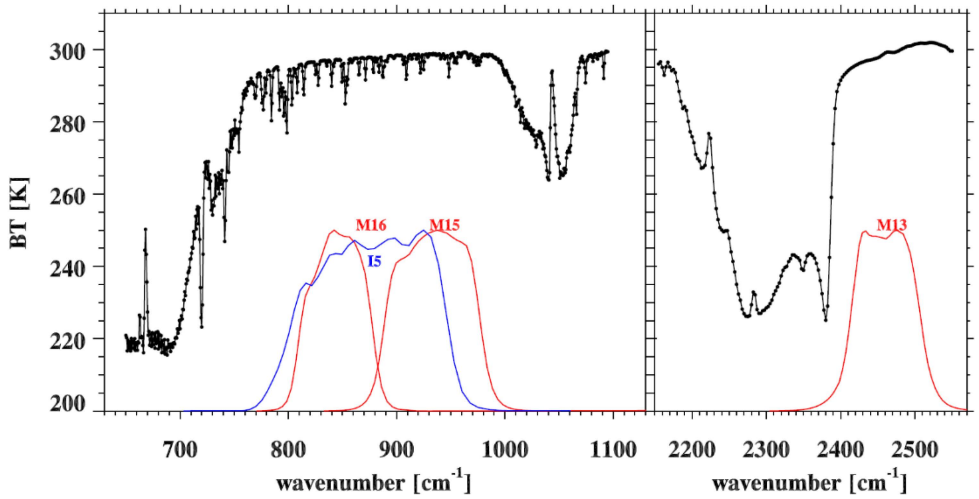

Figure 1. CrIS spectra from the LWIR and SWIR bands (bands 1 and 3) and the VIIRS spectral response functions of I5, M13, M15, and M16 bands.

Shown in Figure 2 are examples of CrIS and VIIRS I5 images from 1024UTC to 1032UTC on 5 September 2015 when the SNPP satellites passed over the Red Sea region. The scan characteristics between the imager and sounder are clearly revealed. Basically, with high spatial resolution and continuous scan (6400 pixel per each scan line), VIIRS has the advantage to resolve the details of clouds and surface features. Given the relatively large footprint and "step-and-stare" scan mechanism (30 FORs per each scan and 9 FOVs in each FOR), there are spatial gaps among the FOVs. In addition, due to the different maximum scan angles of CrIS and VIIRS, that is 48.3° *versus* 58.3°, the VIIRS swath is larger than CrIS. As a result, a part of the Earth surface cannot be detected by CrIS (but can be detected by VIIRS). Figure 3 gives the enlarged four scans of CrIS FOV footprints projected on the Earth overlapped with VIIRS I5 image, which are computed using the method by Wang *et al.* [11]. These spatial gaps are clearly shown. In addition, the FOV footprints close to nadir are projected as a circle on the Earth and steadily changed to an ellipse. Specifically, the center FOV (FOV 5) is changed from a 14.0 km circle at nadir into an ellipse with major and minor axes of 43.6 km and 23.2 km at the end of the scan. Finally, the FOV footprints are also rotated with FORs because of the 45-degree mounted scan mirror. Based on Figure 3, the key of collocation of CrIS and VIIRS images is to find the VIIRS pixels within each large CrIS FOVs footprint.

When we compute the FOV footprint, the CrIS detector size is treated as a 0.963° circle. This value is from CrIS engineering packets and also used for CrIS spectral calibration [17]. However, in reality, the CrIS detectors have their own spatial response functions, namely, the spatial distribution of the contributions to the total radiance. The detector spatial response was measured during prelaunch testing. The response function is approximately a Gaussian distribution and is normalized by the peak value. The FOV size of 0.963° actually corresponds to ~41% of the peak response but already collects ~98% of total radiation falling on the detector. In other words, for a typical sounder instrument like CrIS, its spatial response function quickly reaches its peak and then becomes flat. Theoretically, when spatially averaging collocated VIIRS pixels, the spatial response function should be used as

weights [4]. However, the sensitivity test indicated that it is accurate enough to assume spatial response function as a box shape with 0.963° as a cut-off value and the BT differences caused by this assumption are ~0.002 K.

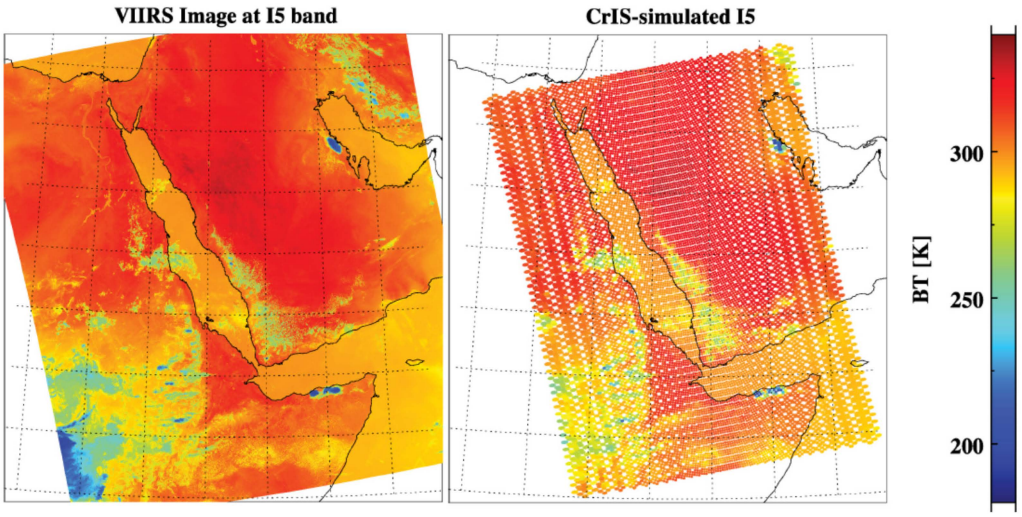

(**a**) (**b**)

Figure 2. Examples of VIIRS I5 (**a**) and CrIS (**b**) images from 1024UTC to 1032UTC on 5 September 2015. The CrIS spectra have been convolved with VIIRS spectral response function to match VIIRS I5 band radiances.

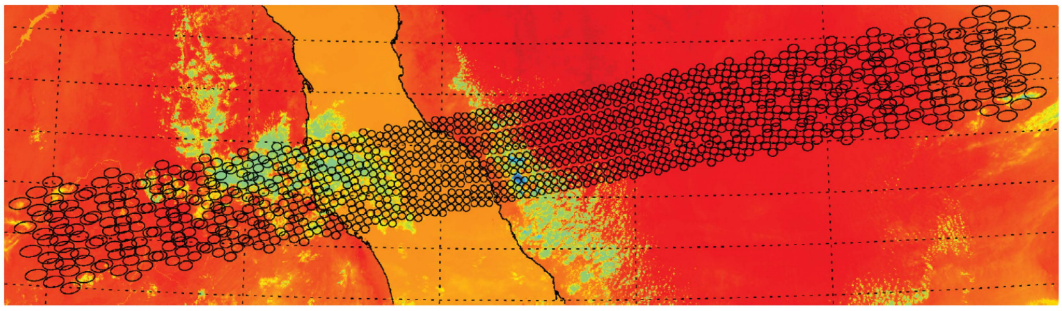

(**a**)

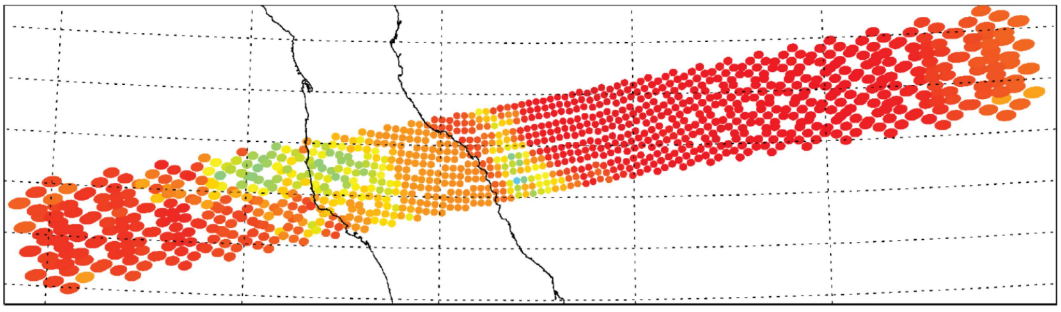

(**b**)

Figure 3. Enlarged plots four CrIS scans in Figure 2, including (**a**) projected CrIS FOV footprints overlapped with VIIRS image and (**b**) CrIS FOV images.

3. Method

The uniqueness of this study is to collocate the VIIRS and CrIS measurements based on VIIRS and CrIS Line-of-Sight (LOS) pointing vectors, defined as the vector from the satellite position to the Earth surface pixel location. As a first step, CrIS and VIIRS geolocation datasets, which contain latitude, longitude, satellite range, satellite azimuth and zenith angles of CrIS and VIIRS measurements, are used to compute the LOS Pointing Vectors. In the following step, VIIRS and CrIS LOS vectors are matched by examining the angle between them. The corresponding indexes of VIIRS pixels are retrieved through the matched VIIRS LOS vectors. The details of the method as well as the optimization and implementation of the algorithm are described in this section.

3.1. Computation of Line-of-Sight (LOS) Pointing Vector

3.1.1. Coordinate Systems

Table 1 and Figure 4 summarize the coordinate systems used in this study. Geolocation datasets of CrIS and VIIRS contain geodetic latitude and longitude of each satellite measurement, characterizing the intersection location of the LOS pointing vector with the Earth. In a typical geographic coordinate system, geodetic latitude and longitude usually represent horizontal position. The third variable represents the vertical position above the Earth's ellipsoid. Hence, this coordinate system can be simply called the geodetic latitude, longitude, and altitude coordinate system (LLA). The reference Earth ellipsoid can be characterized by the so-called geodetic datum. Both CrIS and VIIRS geolocation algorithms use the World Geodetic System 1984 (WGS84) as a geodetic reference. Finally, we should point out that there are actually two geolocation datasets for VIIRS SDR datasets, that is, the one with terrain correction and the other without terrain correction. The geolocation data without terrain correction are used in order to be consistent with CrIS because CrIS only has a geolocation dataset on the Earth ellipsoid without terrain correction.

Table 1. Summary of coordinate systems used in this study.

Coordinates	Type	Origin	Variables
Local Spherical Coordinate	Spherical	Measurement location	(R, Θ, Φ) R: Range (meter) Θ: Zenith Angle (degree) Φ: Azimuth Angle (degree)
Local East, North, Up (ENU) Coordinate	Cartesian	Measurement Location	(East, North, Up) in meter
Geodetic Latitude, Longitude, and Altitude (LLA) Coordinate	Spherical	Earth Center	(ψ, λ, h) ψ: Geodetic Latitude (degree) λ: Longitude (degree) h: Altitude (meter)
Earth-centered, earth-fixed (ECEF) Coordinate	Cartesian	Earth Center	(X, Y, Z) in meter

Given the location of satellite measurements, the satellite position at a given location can be described in a local spherical coordinate system. Specifically, three variables—including satellite azimuth and zenith angle as well as satellite range (the distance from the pixel location to satellite position)—can accurately determine the satellite position at a given point on the Earth. All of these values are contained in CrIS and VIIRS geolocation datasets. Correspondingly, the local East, North, Up (ENU) Cartesian coordinate system (ENU) is formed from a plane tangent to the Earth's surface fixed to the same specific location, and the east axis is labeled E, the north N, and the up U, by convention. It consists of three numbers: one represents the position along the northern axis, one along the eastern axis, and one represents the vertical position pointing up from a local tangent plane. This

ENU coordinate system is far more intuitive and practical when computing the LOS pointing vector, which is simplified as the inverse satellite position vector—the vector that points from the satellite position to the origin (0, 0, 0) in ENU.

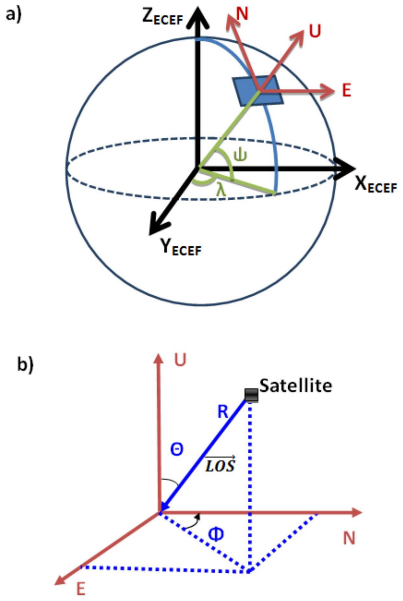

Figure 4. Illustration of the coordinate systems listed in Table 1, including (**a**) ENU (red color), LLA (green color), ECEF (black color) coordinate systems; and (**b**) local spherical coordinate (blue color).

For the local ENU coordinate, however, the origin varies with different satellite measurement locations. It is desirable to choose a common coordinate to show the LOS vector at different locations. Hence, the Earth-Centered, Earth-Fixed (ECEF) coordinate, also known as the Earth Centered Rotational (ECR) coordinate, can be utilized to facilitate the computation. It represents positions as X, Y, and Z coordinates. The point (0, 0, 0) is defined as the center of mass of the Earth, hence the name Earth-Centered. Its axes are aligned with the International Reference Pole (IRP) and International Reference Meridian (IRM) that are fixed with respect to the surface of the Earth. The third axis is formed by the cross product of another two axes. Shown in Figure 5a are three vectors. The satellite position vector **P** is defined as the one pointing towards the satellite from the Earth Center—the ECEF origin. The satellite measurement location vector **G** is the vector pointing towards the location of satellite measurements from the Earth Center. The satellite LOS vector **LOS** is the one pointing towards the satellite measurement location on the Earth Ellipsoid surface from the satellite position. Mathematically, a relationship among these three vectors can be shown as,

$$\boldsymbol{P} = \boldsymbol{G} - \boldsymbol{LOS} \tag{2}$$

Henceforth, except for when the vectors are explicitly denoted in a specific coordinate, they are referred to as those expressed in ECEF. Basically, the collocation CrIS and VIIRS measurements are carried out in ECEF by matching CrIS and VIIRS **LOS** vectors.

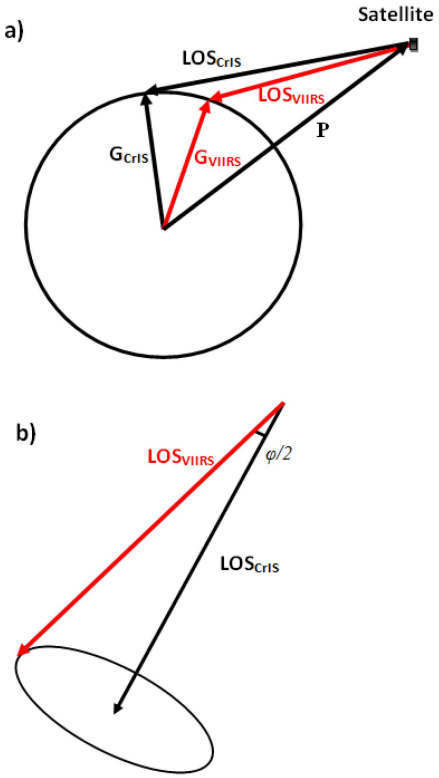

Figure 5. Schematic diagrams showing how to collocate VIIRS pixels CrIS FOV through VIIRS and CrIS LOS pointing vector, including (**a**) computation of the VIIRS and CrIS LOS vectors in ECEF and (**b**) examination of the angle between CrIS and VIIRS LOS vectors. Note that φ is the CrIS detector FOV angle of 0.963°.

3.1.2. Computation of LOS *Vector*

First, given the satellite range, zenith angle, and azimuth angles as (R, Θ, Φ), the $\mathbf{LOS_{ENU}}$ vector in a ENU coordinate can be determined as (E, N, U) as,

$$\boldsymbol{LOS_{ENU}} = \begin{pmatrix} E \\ N \\ U \end{pmatrix} = \begin{pmatrix} R\sin\Theta\sin\Phi \\ R\sin\Theta\cos\Phi \\ R\cos\Theta \end{pmatrix} \tag{3}$$

Second, any vector in a local ENU coordinate can be converted into ECEF through two rotations if we know the geodetic latitude (ψ) and longitude (λ) where the local ENU coordinate is formed, including Equation (1) a clockwise rotation over east-axis by an angle 90-ψ to align the up-axis with the *Z*-axis and then Equation (2) a clockwise rotation over the *Z*-axis by and angle 90+λ to align the east-axis with the X-axis. Consequently, these two rotations can be combined to form the following equation as,

$$\boldsymbol{LOS} = \begin{pmatrix} LOS_X \\ LOS_Y \\ LOS_Z \end{pmatrix} = \begin{pmatrix} -\sin\lambda & -\cos\lambda\,\sin\psi & \cos\lambda\cos\psi \\ \cos\lambda & \sin\lambda\sin\psi & \sin\lambda\cos\psi \\ 0 & \cos\psi & \sin\psi \end{pmatrix} \begin{pmatrix} E \\ N \\ U \end{pmatrix} \tag{4}$$

Finally, the satellite measurement location vector **G** can be computed in ECEF using geodetic latitude (ψ) and longitude (λ) of the satellite measurement location on the Earth ellipsoid

$$\boldsymbol{G} = \begin{pmatrix} G_X \\ G_Y \\ G_Z \end{pmatrix} = \begin{pmatrix} [N(\psi) + h]\cos\psi\cos\lambda \\ [N(\psi) + h]\cos\psi\sin\lambda \\ \left[\frac{b^2}{a^2}N(\psi) + h\right]\sin\psi \end{pmatrix} \quad (5)$$

whereh h is height above the Earth ellipsoid, N(ψ) is Prime Vertical radius of Curvature at a given location that can be computed using geodetic latitude (ψ) as an input, and a and b are semi-major and semi-minor axes for the defined the Earth ellipsoid. For any location on the Earth ellipsoid surface, h simplifies to zero.

Based on the above two steps, the ***LOS*** and ***G*** vectors for CrIS and VIIRS are calculated in ECEF respectively, symbolized as $\boldsymbol{LOS_{VIIRS}}$, $\boldsymbol{LOS_{CrIS}}$, $\boldsymbol{G_{VIIRS}}$, and $\boldsymbol{G_{CrIS}}$. Using Equation (2), the satellite position vector $\boldsymbol{P_{VIIRS}}$ and $\boldsymbol{P_{CrIS}}$ can be further derived. On the other hand, the satellite position vectors in ECEF in the mid scan are saved in the CrIS and VIIRS geolocation dataset when the geolocation algorithm outputs the latitude, longitude, and other geolocation information. Inter-comparison of these two satellite position vectors—the one derived using the above method and the other saved in datasets—can indirectly evaluate the accuracy of the computation method. Shown in Figure 6 is the magnitude of these two satellite position vectors varying with time. Basically, it clearly shows that they are aligned each other over time. The bottom panel gives the magnitude differences of these two satellite position vectors, which are less than 4.0 m (compared to ~7200 km). It confirms that the above method is very accurate and the uncertainties are at a negligible level.

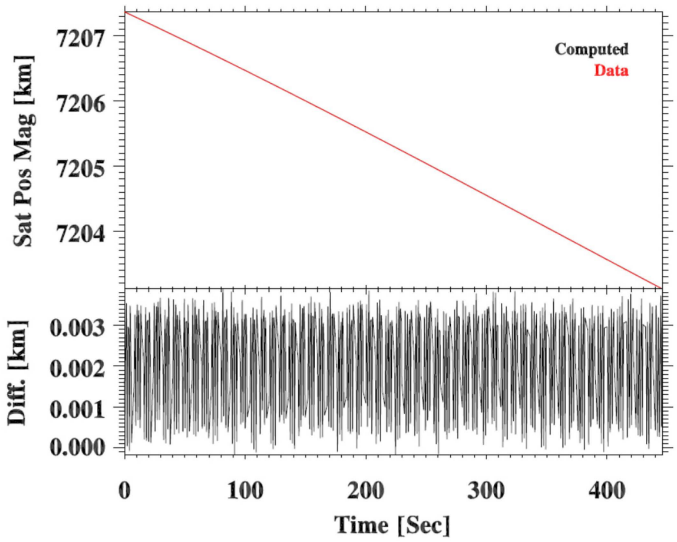

Figure 6. (**Top**) Magnitudes from satellite position vectors in ECEF contained in CrIS geolocation datasets (red color) and derived from Equation (2) (black) as well as their differences (**bottom**).

3.2. Collocation of VIIRS and CrIS LOS Vectors

Once the CrIS and VIIRS LOS vectors are derived, the collocation of VIIRS and CrIS can be simplified as examining the angles between two vectors. As shown in Figure 5b, the circular CrIS detector "sees" the Earth through a solid angle like a cone, whose angular opening is determined by the size of the FOV angle (that is 0.963° for CrIS). Coming from the same satellite position, any VIIRS vectors falling in the cone will overlap with CrIS measurements on the ground. Therefore, we need not be concerned with the size and shape of FOVs on the Earth surface. Generally, the dot product of two Euclidean vectors **A** and **B** is defined by $\boldsymbol{A} \cdot \boldsymbol{B} = ||\boldsymbol{A}||\,||\boldsymbol{B}||\cos\boldsymbol{\theta}$, where θ is the angle of the two

vector and $||\boldsymbol{A}||$ means the length of the vector **A**. Specifically, the criterion for collocation—which determines whether the angle of two vectors is less than a threshold—can be expressed as

$$\frac{(\boldsymbol{G}_{CrIS} - \boldsymbol{P}_{CrIS}) \cdot ((\boldsymbol{G}_{VIIRS} - \boldsymbol{P}_{CrIS})}{||\boldsymbol{G}_{CrIS} - \boldsymbol{P}_{CrIS}|| \, ||\boldsymbol{G}_{VIIRS} - \boldsymbol{P}_{CrIS}||} > \cos\left(\frac{1}{2}\varphi\right) \tag{6}$$

where $\mathbf{G_{CrIS}}$-$\mathbf{P_{CrIS}}$ equals the CrIS LOS vector, $\mathbf{G_{VIIRS}}$-$\mathbf{P_{CrIS}}$ represents the VIIRS LOS vector, and ϕis the FOV size angle of 0.963°. In Equation (6), the numerator is the dot product of the two vectors, while the denominator is the product of the two vectors' lengths. The VIIRS LOS vector has to be re-computed using the same satellite position $\mathbf{P}_{\mathrm{CrIS}}$ from CrIS instead of $\mathbf{P}_{\mathrm{VIIRS}}$ from VIIRS in order to ensure the two vectors of $\mathbf{G_{VIIRS}}$-$\mathbf{P_{CrIS}}$ and $\mathbf{G_{CrIS}}$-$\mathbf{P_{CrIS}}$ originate from the same position. Since there is still a slight time difference between CrIS and VIIRS measurements, the satellite positions for CrIS and VIIRS are not exactly the same. Furthermore, Equation (6) also avoids using an arccosine routine because it needs high accuracy for a small angle between two nearly parallel vectors.

Equation (6) seems straightforward mathematically and is simple to implement computationally. However, the situation is complicated by the fact that one has to go through time-consuming search loops. For examples, in the granule shown in Figure 2, there are 9 × 30 × 56 CrIS FOVs and 6400 × 9216 VIIRS pixels. For a specific CrIS LOS vector corresponding to a CrIS measurement, one has to check whether the angles of this CrIS LOS vector satisfy the requirement stated in Equation (6) with all 6400 × 9216 VIIRS LOS vectors. It turns out there are a total of 9 × 30 × 56 × 6400 × 9216 loops. In computer sciences, it is called brute-force search, which is a very general problem-solving technique that consists of systematically enumerating all possible candidates for the solution and checking whether each candidate satisfies the problem's statement. While a brute-force search is simple to implement, and will always find a solution if it exists, its cost is proportional to the number of candidate solutions in terms of computing time or memory space.

One way to speed up the brute-force search is to reduce the search space, *i.e.*, the set of searched VIIRS pixels. For example, if the search is only limited to near neighbor VIIRS pixels that are close to a given CrIS measurement, the number of loops will be greatly reduced. The main idea is to pre-process the data set, and selectively obtain a set of pivot pixels. The brute-force search is only applied to these pixels to check if they meet the search requirements. To achieve this, the closest VIIRS pixel that matches a given CrIS FOVs location must be first found as a pivot point to define the search area, which may not be necessarily accurate but has to be close enough to the given CrIS FOV. Once this pixel was found, a rectangle area can be defined composed of 201 × 201 VIIRS pixels centered at this VIIRS pixel position. Consequently, the search area is reduced to 201 × 201 VIIRS pixels by trimming out the vast majority of possible search area from original 6400 × 9216 VIIRS pixels.

Finding the closest matched VIIRS pixels for a specific CrIS measurement in the latitude and longitude coordinate system becomes a nearest-neighbor search (NNS) problem. There are various solutions to the NNS problem that have been proposed in computer science. The quality and usefulness of the algorithms are determined by the time complexity of queries as well as the space complexity of any search data structures that must be maintained. For our purpose, the match_2d function [18] is used to find the closest coordinate match between CrIS and VIIRS based on latitude and longitude datasets within a certain search radius. Specifically, a histogram is created to bin the latitude and longitude of VIIRS pixels. The function then searches for ones which have fallen in that bin as well as the relevant three adjacent bins (depending on location within the bin), and finally finds the closest match position. Through the above two considerations, the performance of the collocation algorithm is dramatically improved. For example, on a linux machine with 16 CPUs of 2400.198 MHz, the collocation algorithms for a typical CrIS granule (composed by 9 × 30 × 4 measurements)—which also includes input and output (IO) time—only takes ~8 s.

4. Results and Application

4.1. Collocation Results

The collocation method is applied to the CrIS and VIIRS images shown in Figure 3. The final collocation results are given in Figure 7a, where only VIIRS pixels falling within CrIS FOVs are shown. By way of illustration, Figure 7b shows enlarged collocation plots of FOR1 and FOR15 that have scan angles of -48.3° and -1.65°, respectively. Using the center FOV (FOV5) as an example, it collects 1068 and 3946 VIIRS pixels at scan angles of $-1.65^\circ$and -48.3° and resistively (the blow-tie deleted pixels are not counted). Notice that as the CrIS scan angle increases, the projected CrIS FOVs become increasingly more quasi-elliptical. More importantly, the nine FOVs in given FORs at large scan angles (e.g., FOR 1 and 30) are not exactly identical but also slightly vary with position relative to the FOR center.

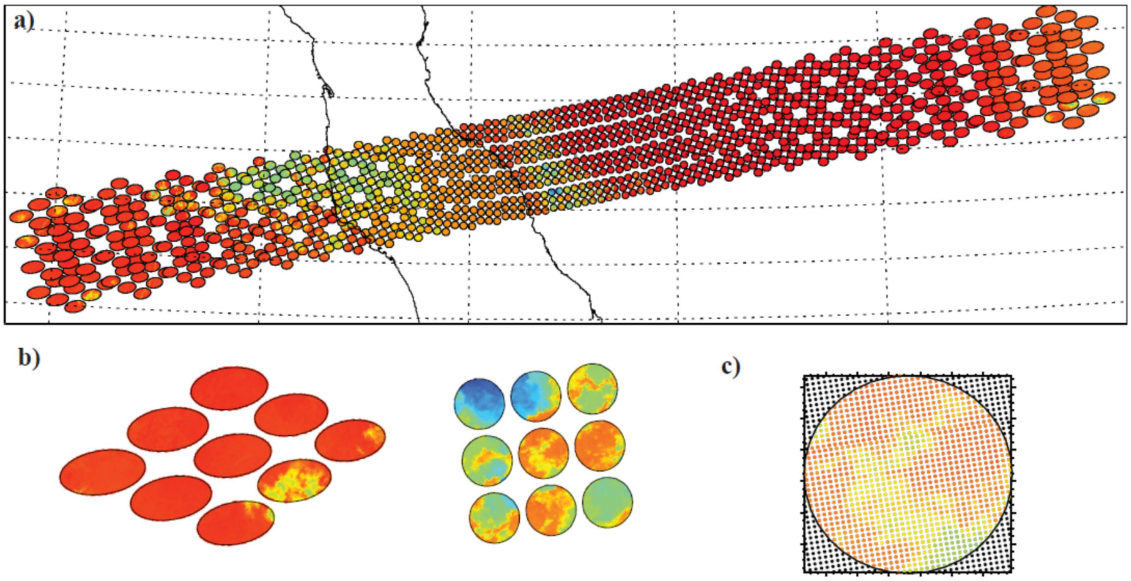

Figure 7. Collocated VIIRS pixels within the CrIS FOVs, including (**a**) the four scans shown in Figure 3; (**b**) the enlarged images for FOR 1 and 15 in the first scan line (from the bottom up) with scan angles of -48.3° and -1.65°; and (**c**) the enlarged plot for the center FOV (FOV 5) in the FOR 15 in the first scan, where the colorful points indicate VIIRS pixels falling within the CrIS FOV and the black ones represent those outside CrIS FOVs. Note that CrIS FOV shapes shown as black lines are independently computed using CrIS geolocation dataset and the FOV angle of 0.963°.

4.2. Collocation Method Evaluation

The accuracy of the collocation is affected by two factors, including Equation (1) the accuracy of collocation method and Equation (2) the accuracy of inputs, e.g., the consistency and accuracy of VIIRS and CrIS geolocation datasets. The latter case is not discussed here because the accuracy of VIIRS and CrIS geolocation data has been discussed in previous studies [11,19]. Therefore, we mainly focus on the former one. In other words, we simply assume that the CrIS and VIIRS geolocation dataset is accurate enough and evaluate the collocation method itself.

Figure 6 indirectly estimates the uncertainties of retrieving CrIS and VIIRS LOS vectors, which are in the order of meters (less than 4.0 m). In the algorithm, we use the double precision approach to perform all the calculations. The final accumulated uncertainties for the collocation method are estimated to be less than 20.0 m. Figure 7c shows the enlarged plots for the center FOV (FOV 5) in the FOR 15 in the first scan, where the colorful points indicate VIIRS pixels falling within the CrIS FOV and the black ones represent those outside CrIS FOVs based on our collocation method. Note that CrIS

FOV shapes shown as black lines are independently computed using CrIS geolocation dataset and the FOV angle of 0.963°. The two independent methods that use the same inputs are consistent with each other, suggesting that the collocation method works well.

The VIIRS radiances values within CrIS FOVs can be spatially averaged together and then compared with CrIS-simulated VIIRS I5 band radiances. It can evaluate the effectiveness and accuracy of the collocation. Shown in Figure 8 are CrIS-VIIRS BT difference maps and a scatter plot of spatial-averaged VIIRS BTs *versus* spectral-convolved CrIS BTs for VIIRS I5 band. If the collocation of CrIS and VIIRS is not accurate enough, the BT differences are expected to have large standard deviations for inhomogeneous scenes because these scenes are very sensitive to spatial match. As a result, these FOVs can be apparently identified from CrIS-VIIRS BT difference map.

Shown in Figure 8, most of the cloudy FOVs and FOVs near coast regions are hard to detect by eyes. Moreover, the scatter plot of CrIS BT *versus* VIIRS BT indicates small standard deviations (spread), suggesting that the collocation method is accurate. On the other hand, the accurate collocation between CrIS and VIIRS allows inter-calibration between the narrow-band imager and hyperspectral sounder to examine each sensor's radiometric calibration [10,20]. The scatter plot in Figure 8 indicates good agreement between CrIS and VIIRS I5 bands, though CrIS is slightly warmer than VIIRS. Demonstrated in Figure 9 is another case that occurred at the North Polar regions on 1 October 2015 and had complicated cloud structures. However, the CrIS-VIIRS BT difference map does not show the corresponding cloud structures, indicating that the collocation method works well.

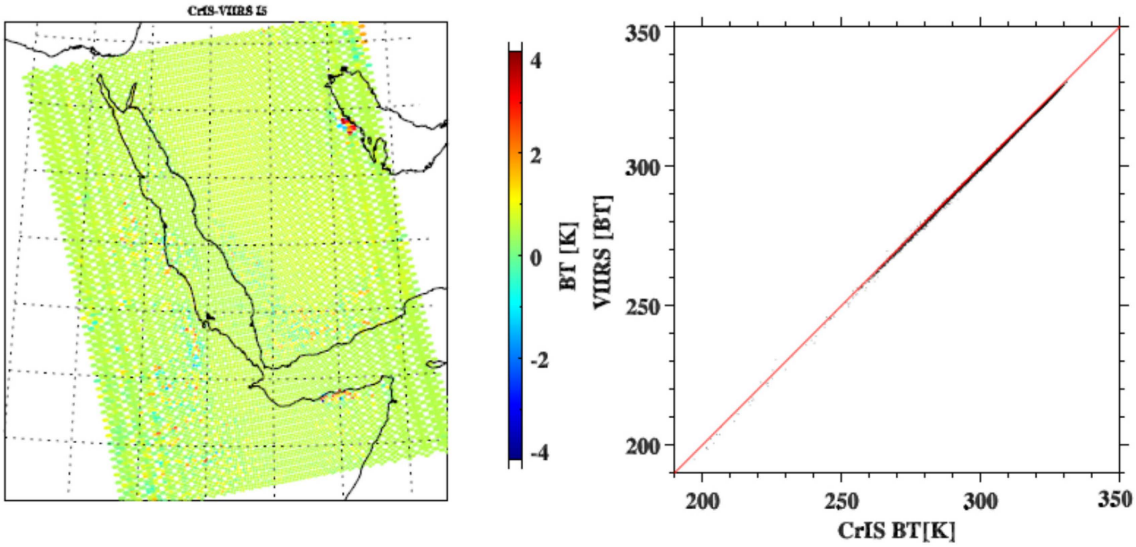

Figure 8. CrIS-VIIRS BT difference image map (**a**) and scatter plot of VIIRS BT *versus* CrIS BT for VIIRS I5 band (**b**). CrIS spectra are convolved with VIIRS SFRs to simulate VIIRS I5 band radiances, while collocated VIIRS radiances are spatially averaged within CrIS FOVs. The original CrIS and VIIRS images can be found in Figure 2.

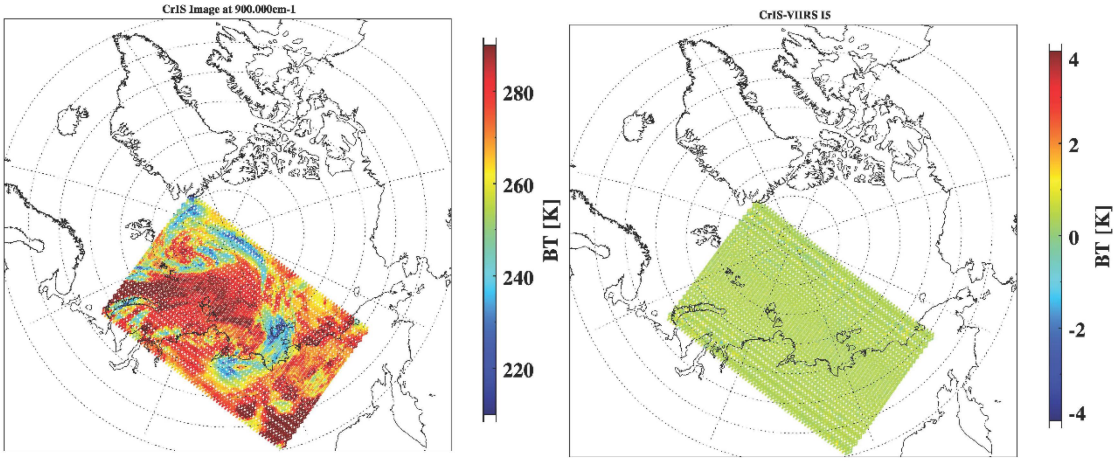

(**a**) (**b**)

Figure 9. CrIS image (**a**) at the North Polar Region on 1 October 2015 and CrIS-VIIRS BT difference map (**b**).

4.3. Other Applications

Another application of collocating VIIRS and CrIS measurements is to characterize CrIS FOV scene features by taking advantage of various VIIRS products. For example, the operational data assimilation of hyper-spectral radiances for numerical weather prediction (NWP) models still relies primarily on cloud-free data, even though substantial progress in the widely studied subject of assimilation of cloud-affected radiances has been made [5]. One challenge remaining in the assimilation of cloud-free infrared sounder radiances is to detect clear and cloud contaminated data correctly. With the fast and accurate collocation of CrIS and VIIRS, one way to identify CrIS clear FOVs is to use a collocated VIIRS cloud mask product (VCM). The VCM technique incorporates a number of cloud detection tests and produces a cloud confidence indicator of confidently cloudy, probably cloudy, probably clear, or confidently clear [21]. Specifically, in order to identify clear sky CrIS FOVs, the VCM products are first collocated with CrIS FOVs using the above collocation method. Second, if all the VIIRS pixels within a given CrIS FOV are all flagged as confidently clear, this CrIS FOV is identified as a clear sky FOV. After the CrIS granule in Figure 2 is examined, 7948 of 15,120 CrIS FOVs are identified as clear sky, shown in Figure 10. Compared with the widely-used observation minus background (O-B) method by the data assimilation community [22], we do believe that the imager-collocated cloud-detection scheme has several advantages. First, it does not rely on model background information as well as radiative transfer calculations. Second, the VIIRS measurements are independent of CrIS and thus can provide reliable sub-pixel information. However, a detailed comparison of these two cloud detection schemes is yet to be finalized.

Finally, we would like to demonstrate that this collocation method can be easily extended to two sensors on different satellite platforms. Shown in Figure 11 are the images from the Atmospheric Infrared Sounder (AIRS) on Aqua and CrIS on SNPP at 900 cm^{-1} on 1 May 2015, when two satellites passed over the western Africa with a ~7-min time difference (Aqua followed SNPP). Since Aqua and SNPP satellites have a similar equatorial crossing time (~1330 LST) but different altitudes (*SNPP*'s altitude is 824 km and *Aqua*'s is 705 km), these two satellites follow each other with a wealth of coincident data through full scan swaths. To collocate CrIS measurements with AIRS measurements using the above method, we only need to replace VIIRS LOS vector with AIRS LOS vector in Equation (6). Basically, the CrIS FOVs that are overlapped with AIRS FOVs are paired together because AIRS and CrIS have a spatial resolution of 13.5 km and 14.0 km at nadir, respectively. In this way, the CrIS FOVs have been re-arranged to spatially match AIRS. The collocated image—which is given in the right panel in Figure 11—looks reasonable. However, we should point out that, for a pair

of sensors on different satellites, the collocation does suffer observational time differences and angle differences. Particularly, for the collocated image shown in Figure 11, the zenith angle differences for collocated FOVs vary from 1.0° to 27° dependent on scan positions.

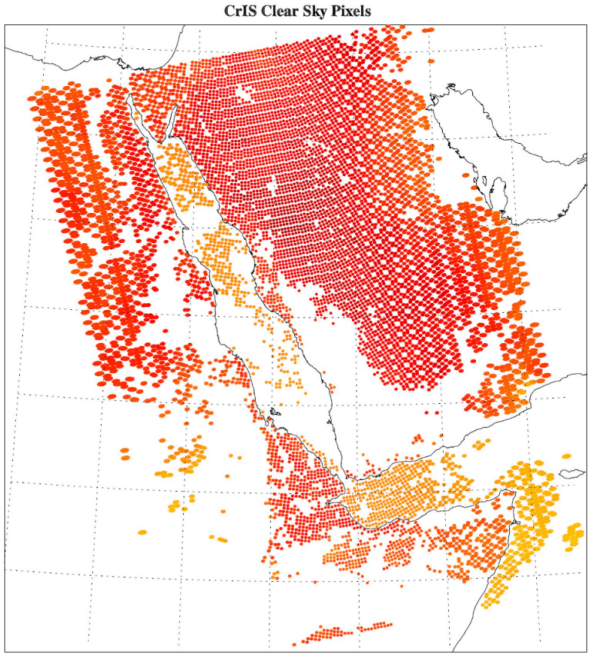

Figure 10. CrIS clear sky FOVs' BTs detected using VIIRS cloud mask product. The original CrIS and VIIRS images as well as the color bar can be found in Figure 2.

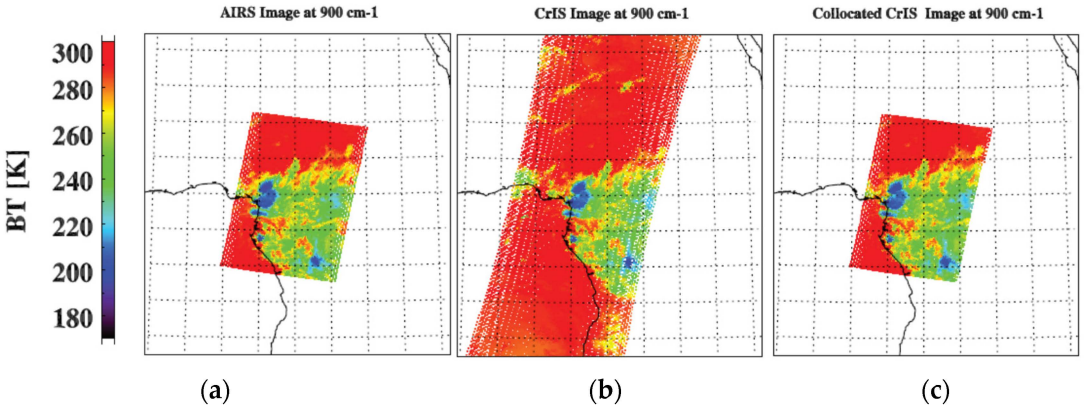

Figure 11. Examples of CrIS (**a**) and AIRS (**b**) images at 900 cm^{-1} as well as a collocated CrIS image that matches AIRS (**c**).

5. Conclusions

Combining high spatial resolution measurements from an imager and high spectral resolution measurements from an IR sounder can greatly improve atmospheric and surface geophysical parameter retrievals, data utilization for numerical weather prediction models, and inter-calibration capabilities including both radiometric and geometric calibration. All these applications depend on an accurate and fast collocation scheme. In this study, a fast and accurate collocation scheme to collocate VIIRS products and measurements with CrIS is developed and discussed in detail, which can be used in the current SNPP and future JPSS satellite platforms. Directly based on the CrIS and VIIRS LOS pointing vectors, the algorithm is mathematically very accurate. More importantly, with optimization, this

method is very fast and efficient and thus can meet operational requirements. We also demonstrate that this collocation method can be extended to a wide variety of sensors on different satellites, for example CrIS with AIRS on different polar orbiting satellites as well as CrIS and geostationary imagers.

As a final note, we would like to point out that the algorithm can be implemented in any language (such as Fortran, Java Python, and C++) that is able to incorporate vector and matrix algebra calculations. It is also feasible to use a nearest-neighbor search in implementing the algorithm in order to respond to operational requirements. Efforts are being made to integrate this algorithm into the operational environments of various applications.

Acknowledgments: The VIIRS and CrIS data for this paper were downloaded at NOAA's Comprehensive Large Array Data Stewardship System. The AIRS data are available at NASA Goddard Earth Sciences (GES) Data and Information Services Center (DISC). The authors thank anonymous reviewers for providing valuable comments for the study. This study is funded by the NOAA JPSS Program Office. Likun Wang is supported by NOAA grant NA14NES4320003 (Cooperative Institute for Climate and Satellites) at the University of Maryland/ESSIC. The manuscript contents are solely the opinions of the authors and do not constitute a statement of policy, decision, or position on behalf of NOAA or the U.S. government.

Author Contributions: Likun Wang is the main author of this research work and wrote the manuscript. Denis Tremblay developed the original version of CrIS footprint shape computation codes in Matlab. Bin Zhang reviewed the IDL collocation codes and identified several bugs. All the authors reviewed and edited the manuscript.

Conflicts of Interest: The authors declare no conflict of interest.

References

1. Cao, C.; Xiong, J.; Blonski, S.; Liu, Q.; Uprety, S.; Shao, X.; Bai, Y.; Weng, F. Suomi NPP VIIRS sensor data record verification, validation, and long-term performance monitoring. *J. Geophys. Res. Atmos.* **2013**, *118*. [CrossRef]
2. Han, Y.; Revercomb, H.; Cromp, M.; Gu, D.; Johnson, D.; Mooney, D.; Scott, D.; Strow, L.; Bingham, G.; Borg, L.; *et al*. Suomi NPP CrIS measurements, sensor data record algorithm, calibration and validation activities, and record data quality. *J. Geophys. Res. Atmos.* **2013**, *118*. [CrossRef]
3. Li, J.; Menzel, W.P.; Sun, F.; Schmit, T.J.; Gurka, J. AIRS subpixel cloud characterization using MODIS cloud products. *J. Appl. Meteorol.* **2004**, *43*, 1083–1094. [CrossRef]
4. Kahn, B.H.; Fishbein, E.; Nasiri, S.L.; Eldering, A.; Fetzer, E.J.; Garay, M.J.; Lee, S.-Y. The radiative consistency of atmospheric infrared sounder and moderate resolution imaging spectroradiometer cloud retrievals. *J. Geophys. Res.* **2007**, *112*, D09201. [CrossRef]
5. Eresmaa, R. Imager-assisted cloud detection for assimilation of infrared atmospheric sounding interferometer radiances. *Q. J. R. Meteorol. Soc.* **2014**, *140*, 2342–2352. [CrossRef]
6. Wang, L.; Wu, X.; Goldberg, M.; Cao, C.; Li, Y.; Sohn, S.-H. Comparison of AIRS and IASI radiances using GOES imagers as transfer radiometers toward climate data records. *J. Appl. Meteor. Climatol.* **2010**, *49*, 478–492. [CrossRef]
7. Wang, L.; Cao, C. On-orbit calibration assessment of AVHRR longwave channels on MetOp-A using IASI. *IEEE Trans. Geosci. Remote Sens.* **2008**, *46*, 4005–4013. [CrossRef]
8. Tobin, D.C.; Revercomb, H.E.; Moeller, C.C.; Pagano, T.S. Use of atmospheric infrared sounder high–spectral resolution spectra to assess the calibration of moderate resolution imaging spectroradiometer on EOS Aqua. *J. Geophys. Res. Atmos.* **2006**, *111*. [CrossRef]
9. Schreier, M.M.; Kahn, B.H.; Eldering, A.; Elliott, D.A.; Fishbein, E.; Irion, F.W.; Pagano, T.S. Radiance comparisons of MODIS and AIRS using spatial response information. *J. Atmos. Oceanic Technol.* **2010**, *27*, 1331–1342. [CrossRef]
10. Wang, L.; Han, Y.; Tremblay, D.; Weng, F.; Goldberg, M. Inter-comparison of NPP/CrIS radiances with VIIRS, AIRS, and IASI: A post-launch calibration assessment. *Proc. SPIE* **2012**, *8528*. [CrossRef]
11. Wang, L.; Tremblay, D.A.; Han, Y.; Esplin, M.; Hagan, D.E.; Predina, J.; Suwinski, L.; Jin, X.; Chen, Y. Geolocation assessment for CrIS sensor data records. *J. Geophys. Res. Atmos.* **2013**, *118*, 690–704. [CrossRef]
12. Cao, C.; Xu, H.; Sullivan, J.; McMillin, L.; Ciren, P.; Hou, Y.-T. Intersatellite radiance biases for the high-resolution infrared radiation sounders (HIRS) on board NOAA-15, -16, and -17 from simultaneous nadir observations. *J. Atmos. Ocean. Technol.* **2005**, *22*, 381–395. [CrossRef]

13. Holl, G.; Buehler, S.A.; Rydberg, B.; Jimenez, C. Collocating satellite-based radar and radiometer measurements—Methodology and usage examples. *Atmos. Meas. Tech.* **2010**, *3*, 693–708. [CrossRef]
14. Aoki, T. *A Method for Matching the HIRS-2 and AVHRR Pictures of TIROS-N Satellites*; Technical Note for Meteorological Satellite Center: Tokyo, Japan; October; 1980; pp. 15–26.
15. Aoki, T. Clear radiance retrieval of HIRS channels with the use of AVHRR data. In Proceedings of the Technical Proceedings of the First TOVS Study Conference, Igls, Austria, 29 August–2 September 1983.
16. Nagle, F.W.; Holz, R.E. Computationally efficient methods of collocating satellite, aircraft, and ground observations. *J. Atmos. Oceanic Technol.* **2009**, *26*, 1585–1595. [CrossRef]
17. Strow, L.; Motteler, H.; Tobin, D.; Hannon, S.; Predina, J.; Suwinski, L. Frequency calibration and validation of CrIS satellite sounder. *J. Geophys. Res. Atmos.* **2013**, *118*, 12486–12496. [CrossRef]
18. Match_2d Function. Available online: http://tir.astro.utoledo.edu/idl/match_2d.pro (accessed on 20 January 2016).
19. Wolfe, R.E.; Lin, G.; Nishihama, M.; Tewari, K.P.; Tilton, J.C.; Isaacman, A.R. Suomi NPP VIIRS prelaunch and on-orbit geometric calibration and characterization. *J. Geophys. Res. Atmos.* **2013**, *118*. [CrossRef]
20. Tobin, D.; Revercomb, H.; Knuteson, B.; Best, F.; Taylor, J.; Deslover, D.; Borg, L.; Moeller, C.; Martin, G.; Kuehn, R.; *et al*. Soumi NPP/JPSS Cross-Track Infrared Sounder (CrIS): Intercalibration with AIRS, IASI, and VIIRS. In Proceedings of the 93rd AMS Annual Meeting, Austin, TX, USA, 6–10 January 2013.
21. Kopp, T.J.; Thomas, W.; Heidinger, A.K.; Botambekov, D.; Frey, R.A.; Hutchison, K.D.; Iisager, B.D.; Brueske, K.; Reed, B. The VIIRS cloud mask: Progress in the first year of S-NPP toward a common cloud detection scheme. *J. Geophys. Res. Atmos.* **2014**, *119*, 2441–2456. [CrossRef]
22. McNally, A.P.; Watts, P.D. A cloud detection algorithm for high-spectral-resolution infrared sounders. *Q. J. R. Meteorol. Soc.* **2003**, *129*, 3411–3423. [CrossRef]